The EUMETSAT Network of Satellite Application Facilities

GRAS SAF
GRAS Meteorology

EUMETSAT Satellite Application Facility on GRAS Meteorology

CDOP Visiting Scientist Report 6:
Upgrading of OCC code for operational processing of GRAS raw sampling data

Version 1.0

26 October 2009

Danish Meteorological Institute (DMI)
European Centre for Medium-Range Weather Forecasts (ECMWF)
Institut d'Estudis Espacials de Catalunya (IEEC)
Met Office (MetO)

Ref: SAF/GRAS/DMI/MGT/CVS06/003

DOCUMENT AUTHOR TABLE

	Author(s)	*Function*	*Date*	*Comment*
Prepared by:	Michael Gorbunov	GRAS SAF VS	26/10/2009	
Reviewed by:				
Approved by:	Kent Bækgaard Lauritsen	GRAS SAF Project Manager	26/10/2009	

DOCUMENTATION CHANGE RECORD

Issue / Revision	*Date*	*By*	*Description*
1.0	21/10/09	MEG	First version.

Processing GRAS data: algorithms and results

M.E. Gorbunov

Obukhov Institute for atmospheric physics
Russian Academy of Sciences,
Pyzhevsky per. 3, Moscow 119017, Russia

Contents

1. Reading GRAS Data

1.1 Recognition of GRAS Data

Program OCC has been modified to be able to recognize and read GRAS data in the NetCDF format. Currently, the program can automatically recognize and process GPS/MET data, CHAMP data in RINEX format, GPS/MET and CHAMP data in NetCDF-based atmPhs format (supplied by UCAR), COSMIC data in atmPhs format, GRAS data in NetCDF format, and simulated data in LEO-LEO format. The latter is a RINEX-like ASCII format of occultation data with a variable number of channels developed by M. E. Gorbunov for numerical simulations of LEO-LEO multichannel radio occultation measurements.
The recognition algorithm is based on reading the first 8 bytes of the file. The bytes are checked for the presence of the RINEX or NetCDF signature. If the NetCDF signature is found, an attempt is made to open the file as a NetCDF file using the standard NetCDF library (supplied in the form of the source code). If the file is successfully opened, the program tries to read global attribute `"title"`. If the attribute is successfully read, its value is compared with the text string `"MetOp-A / GRAS radio occultation data"`. If the result of this comparison is positive, the file is assigned data type GRAS-NetCDF, and the subroutine for reading this data format is invoked.

1.2 Extracting and Converting Basic Variables

From a GRAS NetCDF file, the subroutine reads all the variables necessary for the inversion of radio occultation data. Attempt of reading each variable is followed by checking the error code returned by the corresponding member of NetCDF library. If any operation returns a non-zero error code, the subroutine returns the `"missing variable"` error code and exits, and the main program issues a diagnostic message and stops.
The subroutine starts with obtaining the dimensions of the closed loop (CL) and raw sampling (RS) records, N_{CL} and N_{RS}, respectively. Then the starting time of the event, represented by variables `start_time_absdate` (absolute date of the beginning of the event in the days since 0001-01-01 00:00:00.00 computed using the Gregorian calendar) and `start_time_abstime` (time of the beginning of the event in seconds since 00:00:00.00 of the event beginning date) are read. The values of `start_time_absdate` and `start_time_abstime` are converted to year, month, day, hour, minute and second, which represent the occultation start time. Then arrays of relative time CL and RS times, `cl_dtime` t_i^{CL} and `rs_dtime` t_j^{RS} (seconds from the beginning of the event) are read.
The coordinates and velocities of GNSS and LEO satellites are obtained from variables `cl_r_gns`, `cl_v_gns`, `cl_r_rec`, `cl_v_rec`, `rs_r_gns`, `rs_v_gns`, `rs_r_rec`, and `rs_v_rec`, where `cl` stays for closed loop, and `rs` stays for raw sampling, `r` stays for coordinates, `v` stays for velocity, `gns` stays for the GNSS satellite, `rec` stays for the receiver (LEO). These variables are measured in meters and meters per second. We convert them into kilometers and kilometers per second, which are the preferred measurement units in the environment of program OCC, producing vectors:

- $\mathbf{X}_i^{G,CL}$ (GNSS coordinates for CL record),
- $\mathbf{V}_i^{G,CL}$ (GNSS velocities for CL record),
- $\mathbf{X}_i^{L,CL}$ (LEO coordinates for CL record),

- $\mathbf{V}_i^{L,CL}$ (LEO velocities for CL record),
- $\mathbf{X}_j^{G,RS}$ (GNSS coordinates for RS record),
- $\mathbf{V}_j^{G,RS}$ (GNSS velocities for RS record),
- $\mathbf{X}_j^{L,RS}$ (LEO coordinates for RS record), and
- $\mathbf{V}_j^{L,RS}$ (LEO velocities for RS record).

The L1/L2 amplitudes $A_i^{1,CL}$ and $A_i^{2,CL}$ for the CL record are obtained from variables `cl_snr_ca` and `cl_snr_p2`, respectively. The L1 excess phases $S_i^{1,CL}$ for the CL record are obtained from variable `cl_exphase_ca`.
The L2 excess phases $S_i^{2,CL}$ is computed from variables I_j^{P2} `cl_i_p2`, Q_j^{P2} `cl_q_p2`, representing I- and Q- components of P2 signal, and the excess phase of numerically controlled oscillator (NCO) for L2, `cl_exphase_l2_nco`. The L2 down-converted phase is defined as follows:

$$\varphi_j^{2,CL} = \arg\left(I_j^{P2} + iQ_j^{P2}\right). \tag{1}$$

This phase is accumulated. The accumulation of the phase consists in adding an integer number of cycles at each point in such a way that the absolute variation of the phase is minimized:

$$\begin{aligned} \tilde{\varphi}_1^{2,CL} &= \varphi_1^{2,CL}, \\ \tilde{\varphi}_{j+1}^{2,CL} &= \tilde{\varphi}_j^{2,CL} + \left(\left(\varphi_{j+1}^{2,CL} - \varphi_j^{2,CL} + \pi\right) \bmod 2\pi\right) - \pi. \end{aligned} \tag{2}$$

The L2 excess phase is obtained as follows:

$$S_j^{2,CL} = S_j^{NCO,CL} - \frac{2\pi f_2}{c}\tilde{\varphi}_j^{2,CL}, \tag{3}$$

where f_2 is the L2 frequency. The normalized I- and Q-components of the L1 complex signal, I_j^N and Q_j^N for the RS record are read from variables `rs_i_ca_norm` and `rs_q_ca_norm`. The L1 amplitude $A_i^{1,RS}$ for the RS record is obtained from variables `rs_snr_ca`. L2 signal is missing in the RS mode. The L1 down-converted phase is defined as follows:

$$\varphi_j^{1,RS} = \arg\left(I_j^N + iQ_j^N\right). \tag{4}$$

This phase is accumulated in a way similar to (2) producing connected phase $\tilde{\varphi}_1^{1,RS}$. The NCO excess phase $S_j^{NCO,RS}$, is obtained from variable `rs_exphase_l1_nco`. The L1 excess phase is obtained as follows:

$$S_j^{1,RS} = S_j^{NCO,RS} - \frac{2\pi f_1}{c}\tilde{\varphi}_j^{1,RS}, \tag{5}$$

where f_1 is the L1 frequency.

1.3 Reading Navigation Bits

GRAS data contain two types of navigation bits: external and alternative. The external ones are obtained from the network of ground-based stations. The alternative ones are obtained by identifying phase jumps by π between samples. We use the term “alternative navigation bits” to emphasize that they come from externally supplied files and to distinguish them from the

internal navigation bits obtained by our processing program `OCC`. We only use navigation bits for RS record.

The navigation bits are obtained from variables `rs_navbits_internal` and `rs_navbits_external`. Integer variable `rs_have_navbits_external` may have the value of 1 or 0, indicating whether external navigation bits are, respectively, present or absent in the file. For storing navigation bits we introduce integer variables L_i^{CL} and L_i^{RS}.

These variables are treated bitwise, separate bits having the following meanings (counted from the least significant bit):

- bit 0 (2^0) : 0 = CL mode, 1 = RS mode,
- bit 1 (2^1) : external navigation bits,
- bit 2 (2^2) : external navigation bits quality,
- bit 3 (2^3) : missing data,
- bit 4 (2^4): alternative navigation bits,
- bit 5 (2^5): alternative navigation bits quality,
- bit 6 (2^6): CL overlapping with RS,
- bit 7 (2^7): internal navigation bits,
- bit 8 (2^8): internal navigation bits quality,

If external navigation bits are missing, as indicated by variable `rs_have_navbits_external`, alternative bits are copied into the positions of the external ones. Bits 2 and 5 (navigation bits quality) are always set to 1. Bit 2 may have different values in the processing of COSMIC data, where the files with external navigation bits also contain the navigation bits quality. Internal navigation bits may be computed later during the open-loop data pre-processing, if this is requested by a corresponding command line option.

1.4 Marking Gaps in CL and RS Records

In some of GRAS files, CL and RS records may have gaps. Gaps are identified as intervals between samples, whose length exceeds the minimum interval by 5%. The reading routine marks the gaps. For this purpose, we use bit 3 of variables L_i^{CL} and L_i^{RS}.Two samples surrounding each gap are marked with the flag `"missing data"`.

2. Pre-processing GRAS data

2.1 Merging CL and RS Records

Program `OCC` has an option that controls the mode of merging CL and RS data. Currently, two modes are supported:

1. CL data only;
2. RS data complemented with CL data.

The first mode specifies using CL data only, discarding all the RS records. This mode is necessary for the data validation purposes. In the second mode, the whole RS record is complemented with CL data where no RS are present.

The data are interpolated to an equidistant united time grid. The step of the united grid equals to that of RS time grid, if RS data are used, and to that of CL grid, if using CL data only has been selected.

When using CL data only, the united grid has the minimum and maximum time corresponding to that of the CL time grid.

If RS data are complemented with CL data, the united grid is defined as follows. For rising events, minimum time equals the minimum RS time, and the maximum time equals the maximum CL time, additional anchor point equals the maximum RS time. For setting events, minimum time equals the minimum CL time, and the maximum time equals the maximum RS time, additional anchor point equals the minimum RS time. The anchor points secure that the united grid will cover all the RS grid points, such that the RS excess phase will be copied rather than interpolated. This is necessary to prevent parasitic phase variations when interpolating excess phase in the vicinity of the navigation bit flips.

The CL/RS excess phase, amplitude, and GPS and LEO coordinates and velocities are interpolated to the united grid according to the CL/RS merging mode. Variables L_i^{CL} and L_i^{RS} on the united grid are taken from the nearest CL or RS time grid point.

This procedure produces the united record of GPS/LEO coordinates $\mathbf{X}_i^{G,L}$ and velocities $\mathbf{V}_j^{G,L}$, L1/L2 excess phases $S_i^{1,2}$, L1/L2 amplitudes $A_i^{1,2}$, and navigation bits and flags L_i on the equidistant grid. The record fragments corresponding to gaps in the original CL/RS records are filled-in with interpolated values and marked as missing data.

2.2 Connecting Excess Phase

The resulting excess phase is, generally speaking, not continuous. The contiguous fragments of CL/RS excess phase records between gaps include additive phase constants (presumable, integer number of full cycles) that significantly differ for different fragments. Therefore, the phase needs to be connected.

For this purpose, we generate a rough phase model based on a simple exponential model of bending angle profile. We estimate the maximum bending angle $\varepsilon_{\max}$ by taking the lowest GPS and LEO satellite positions $\mathbf{X}_{i0}^{G,L}$ in the frame centered at the Earth's local curvature center and assuming the minimum impact parameter $p_{\min} = r_E + 1.7$ km, where r_E is the Earth's local curvature radius:

$$\varepsilon_0 = \arccos\frac{\left(\mathbf{X}_{i0}^L, \mathbf{X}_{i0}^G\right)}{\left|\mathbf{X}_{i0}^L\right|\left|\mathbf{X}_{i0}^G\right|} - \arccos\frac{p_{\min}}{\left|\mathbf{X}_{i0}^L\right|} - \arccos\frac{p_{\min}}{\left|\mathbf{X}_{i0}^G\right|}; \tag{6}$$

$$\varepsilon_{\max} = \max\left(0.02 \text{ rad}, \varepsilon_0 + 0.001 \text{ rad}\right).$$

The model bending angle profile is defined as follows:

$$\varepsilon(p) = \varepsilon_{\max} \exp\left(-\frac{p - p_{\min}}{5.0 \text{ km}}\right). \tag{7}$$

Using the excess phase model S_i^M corresponding to this bending angle profile, we compute the down-converted L1 and L2 phases, where data are not marked as missing, as follows:

$$\varphi_i^{1,2} = \frac{c}{2\pi f_{1,2}}\left(S_i^{1,2} - S_i^M\right). \tag{8}$$

Where the data are marked as missing, we set $\varphi_i^{1,2} = 0$. The phase is re-accumulated using an equation similar to (2) producing the continuous down-converted phase $\tilde{\varphi}_i^{1,2}$, and the continuous excess phase is computed:

$$\tilde{S}_i^{1,2} = S_i^M + \frac{2\pi f_{1,2}}{c}\tilde{\varphi}_i^{1,2}. \tag{9}$$

Small gaps of the united record, whose lengths does not exceed 0.04 seconds, are accepted, and the missing data flags are reset for them.

2.3 Data Cut-off

The united record is scanned in the descending order (direct order for setting occultations, and inverse order for rising ones) until the first occurrence of missing data flag marking a gap longer than 0.04 seconds. The record is cut-off here.

2.4 Final Set of Variables

Finally, we obtain the complete set of variables including the following ones:

- t_k (relative time of samples),
- $\mathbf{X}_k^G$ (GNSS coordinates for CL record),
- $\mathbf{V}_k^G$ (GNSS velocities for CL record),
- $\mathbf{X}_k^L$ (LEO coordinates for CL record),
- $\mathbf{V}_k^L$ (LEO velocities for CL record),
- $S_k^{1,2}$ (L1/L2 excess phase),
- $A_k^{1,2}$ (L1/L2 amplitudes),
- L_k (navigation bits and flags).

These are the standard variables similar to those provided for COSMIC, CHAMP or SAC-C satellites by UCAR and GFZ. These variables can be used as the input to any of the existing radio occultation processing systems.

3. Processing GRAS Data

3.1 L1 Preprocessing

The measurements in L1 channel (f_1=1.57542 GHz) are performed in two receiver modes: CL and RS. Closed loop mode is used for tracking signals corresponding to rays with perigee heights above 4–10 km. This height varies for different occultations, it depends upon the region. RS mode is ideal for tracking signals with strong variations of the phase, which are characteristic for the tropospheric propagation.

RS mode is used for ray perigee heights below 4–10 km. The processing of open-loop mode signals requires the navigation bits removal (wipe-off) and phase re-accumulation. Our procedure follows the guidelines of the navigation bits removal outlined in [1, 2].

When using externally supplied (external or alternative) navigation bits, the standard demodulation procedure is employed. According to the navigation bit states, 0 or 1, we add 0 or π to the excess phase samples, then subtract the phase model, re-accumulate the phase, and add the phase model to restore the phase variation. The phase model used for the phase re-accumulation is based on the MSIS climatology with addition of a simple model of humidity: we assume a constant relative humidity of 90% below a height of 15 km, and humidity is set to 0 above 15 km. If necessary, this model is extrapolated using smoothed measurements of the L1 excess phase. As shown in [1], even a rough model of the atmosphere allows for the prediction of the Doppler frequency within 10–15 Hz. This indicates that even for the COSMIC data having the sampling rate of 50 Hz, the ±25 Hz interval around the phase model will cover the spectrum of the signal. For the GRAS data that have a sampling rate of 1000 Hz, even a rougher phase model can be used.

To check the quality of the navigation bits, we apply the correlation approach [4] and form the following two functions (normalized derivatives of the phase and navigation bits):

$$F_i^{\varphi} = \left| \frac{\left(\pi + \varphi_{1,i} - \varphi_{1,i-1}\right) \bmod 2\pi - \pi}{\pi} \right|, \qquad (10)$$

$$F_i^{B} = \left| B_i - B_{i-1} \right|,$$

where $\varphi_{1,i}$ are the L1 phases including the navigation bits modulation and B_i are the navigation bits. The first function, F_i^{φ}, visualizes the changes of the navigation bits in the area where the phase variations between samples are significantly smaller than π, and the large phase variations can be attributed to navigation bits changes. The function should equal 1, where the navigation bit sequence switches from 0 to 1 or from 1 to 0, and it equals 0, where navigation bits do not change. The second function, F_i^{B}, has the same property, but it operates on the recorded navigation bits. We compute the following correlation function:

$$C^{B}(\Delta i) = \frac{\left\langle F_i^{\phi} F_{i+\Delta i}^{B} \right\rangle}{\sqrt{\left\langle \left(F_i^{\phi}\right)^2 \right\rangle \left\langle \left(F_{i+\Delta i}^{B}\right)^2 \right\rangle}}, \qquad (11)$$

where averaging is performed with respect to index i over the time interval of 4 seconds below the upper height of the RS mode region. The correlation maximum position is equal to the eventually necessary shift of the navigation bits sequence. Shifting the navigation bits sequence was found necessary for some of COSMIC events. If the maximum correlation is below some specified level (which can be specified by a command-line option, the default value being 0.4), then the internal navigation bits removal [2] is activated.

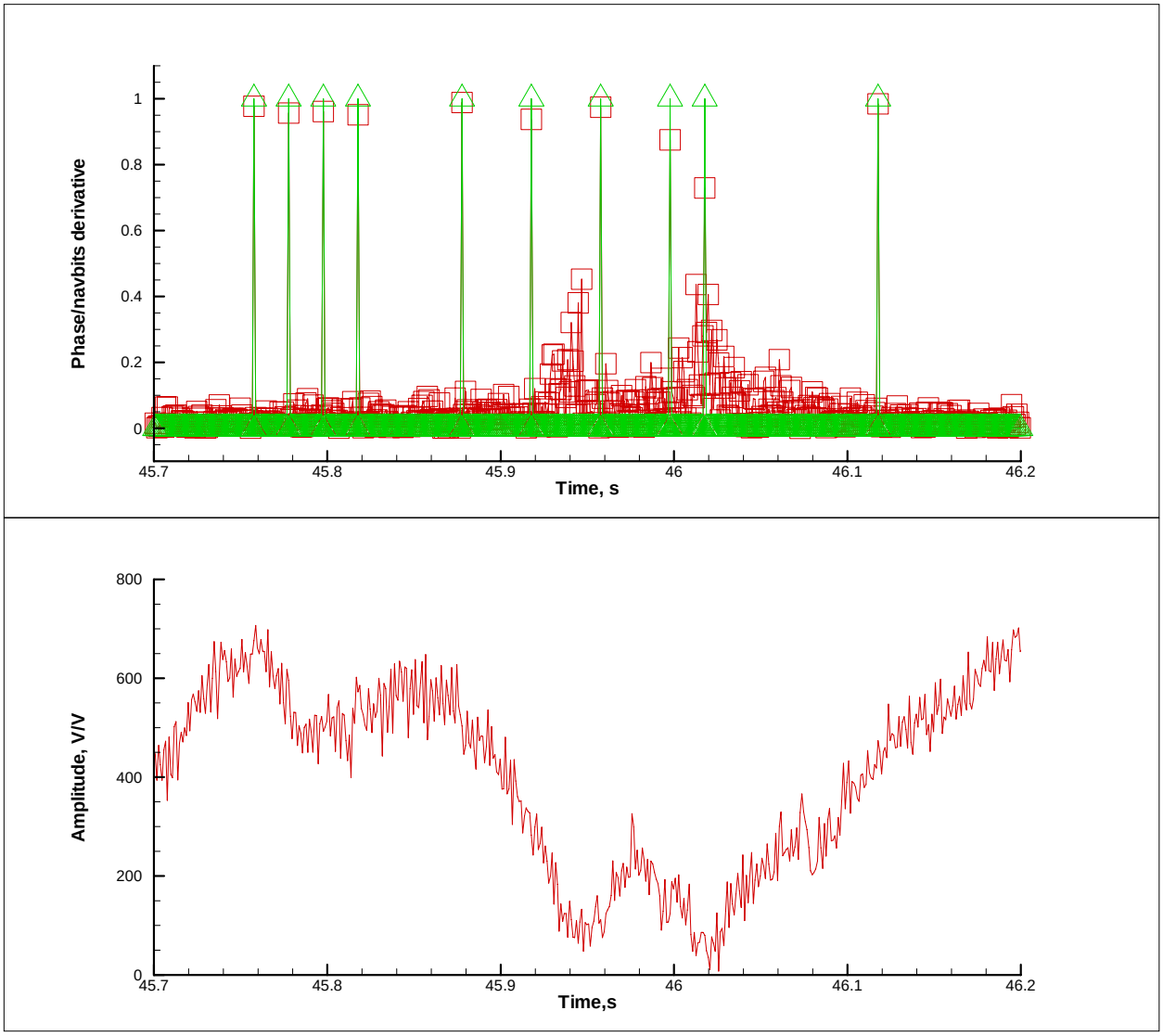

Figure 1. Occultation event at 38.6°S 9.0°W, 2007/09/30, UTC 00:02. Upper panel: normalized derivatives of the phase (red line) and navigation bits (green line). Lower panel: amplitude.

The external navigation bits are not always present in the files. This indicates the necessity of an internal navigation bits demodulation procedure. We follow the guidelines laid-out in [2], with the modifications necessary for processing 1000 Hz data.
Navigation bits have a frequency of 50 Hz, so we find the samples, between which the GPS time crosses an integer number of 0.02 second periods, and only perform the identification of the navigation bits flips here. We implemented the internal navigations bits removal where they are absent or marked as non-reliable, and use the externally-supplied navigation bits otherwise. The internal navigation bits removal imitates the 2-quadrant detector that is insensitive to navigation bits, but cannot effectively track the signal in presence of severe multipath conditions [3]. The internal navigation bits removal consists in a half-cycle re-accumulation of the phase, i.e. in addition of an integer number of half-cycles (π) to the samples of the phase so as to minimize the phase variation between the samples.
In addition to the navigation bits removal, we also apply the half-cycle re-accumulation to L1 phase recorded in the CL mode. There are examples of COSMIC occultations with extra half-

cycles between samples in the CL mode (which is equivalent to ±25 Hz addition to the Doppler frequency). The half-cycle phase accumulation treats half cycles as zeros, and restores the corrupted phase.

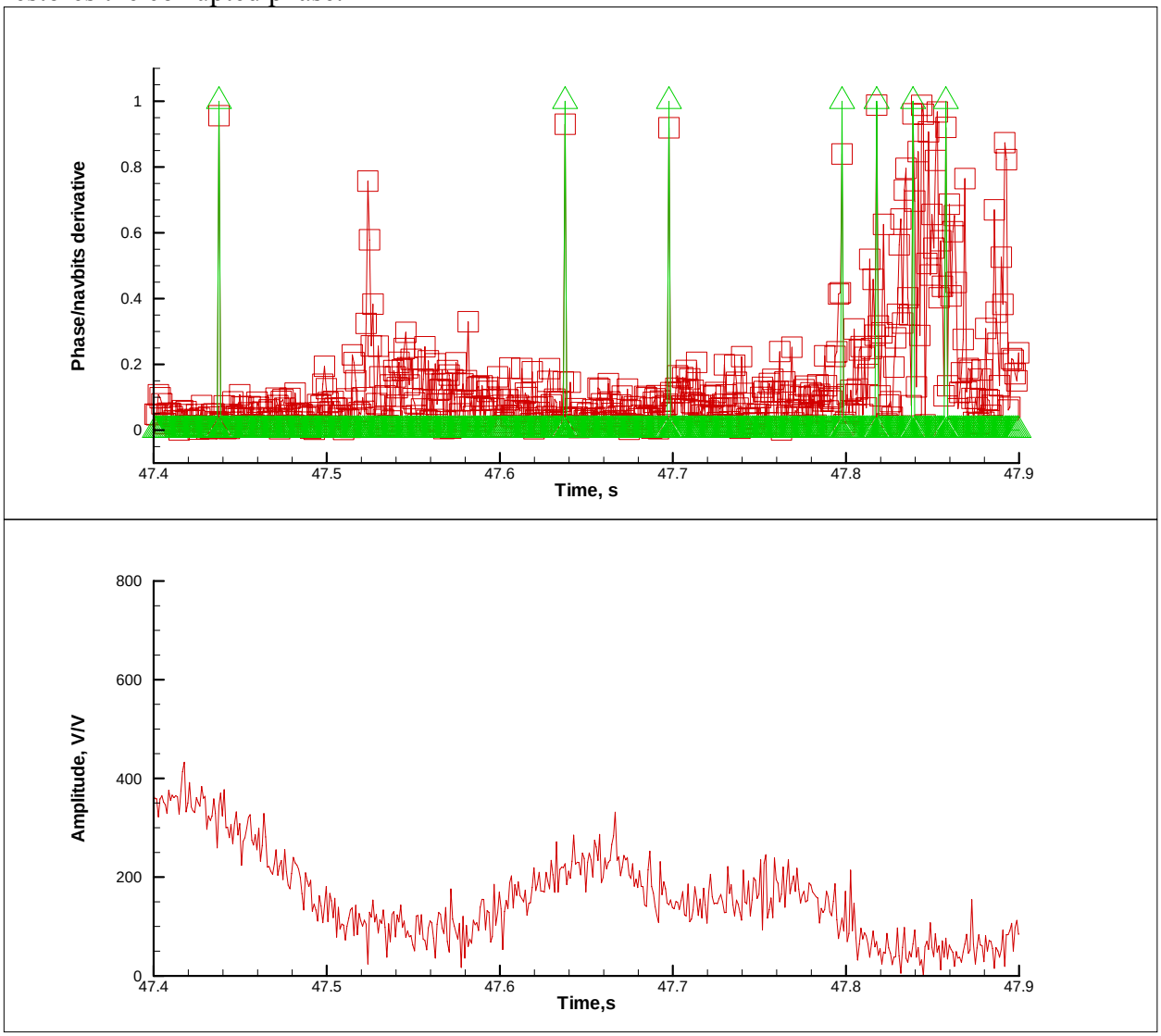

Figure 2. Occultation event at 38.6°S 9.0°W, 2007/09/30, UTC 00:02. Upper panel: normalized derivatives of the phase (red line) and navigation bits (green line). Lower panel: amplitude.

Figure 1 and Figure 2 show examples of normalized derivatives of the phase and navigation bits and the corresponding fragment of the amplitude (SNR) record. The correlation between the phase and navigation bits derivatives depends on the amplitude. For high amplitude the correlation is very good. Where the amplitude drops below the level about 200 V/V, the correlation gets poorer, because the relative noise level increases.

3.2 L2 Preprocessing and Quality Control

Processing of L2 (f_2=1.22760 GHz) excess phase is completely different from processing L1 data due to the following reasons: 1) L2 channel is not operated in RS mode. When the receiver switches to the RS mode, there is no L2 data, some rough phase model is substituted

instead. 2) L2 data are much noisier than L1 data. We use the following scheme of the noise reduction and extrapolation of L2 data.

L2 amplitude is replaced by the smooth geometric optical (GO) amplitude computed for the MSIS model. L2 data is subjected to the radio holographic (RH) filtering in the time domain as described in [5], the L2 excess phase is then pre-filtered with a window 0.25 km. We compute the badness estimate of the L2 signal using the procedure described in [5] with some modifications. Using the radio holographic analysis, we retrieve the smoothed profiles of L1/L2 impact parameter $\overline{p}_{1,2}(t)$, bending angle $\overline{\varepsilon}_{1,2}(t)$, corresponding relative Doppler frequency shift $\overline{d}_{1,2}(t)$, excess phase $\overline{S}_{1,2}(t)$, and the impact parameter spectral widths $\delta p_{1,2}(t)$ [5]. We form the following L2 badness estimate:

$$Q^{L2}(t) = \left(\frac{\left| \overline{p}_1(t) - \overline{p}_2(t) \right|}{\Delta p_A} + \frac{\delta p_2(t)}{\Delta p_D} \right)^2, \qquad (12)$$

where $\Delta p_A = 0.2$ km and $\Delta p = 0.15$ km (these values were found empirically). The badness parameter penalizes data where L1 and L2 impact parameters diverge too much from each other (this corresponds to lost L2 signal track or missing L2 data) and where L2 signal has a large spectral width (this corresponds to noisy L2 data). The discrepancy between L1 and L2 (here represented by the first term in (12) is also employed in the other RO data processing systems [6, 7]. The L2 cut-off point is defined as the highest point of the CL record where $Q^{L2}(t)$ exceeds some threshold Q_0 (which is set to an empirical value of 15), but not higher that the point with the straight-line perigee height of 20 km. If $Q^{L2}(t) < Q_0$ everywhere, then the cut-off point is defined as the lowest point of the CL record.

Below the cut-off point, the L2 data are replaced by extrapolated values. We estimate the ionospheric difference of the bending angles $\Delta\varepsilon_I$ by averaging $\overline{\varepsilon}_2(p) - \overline{\varepsilon}_1(p)$ over the 2 km interval above the cut-off point. The L2 bending angles below the cut-off point are estimated as $\overline{\varepsilon}_1(p) + \Delta\varepsilon_I$, and from them we compute the extrapolated smoothed L2 excess phase $\overline{S}_2^{ext}(t)$. The ionospheric difference of the excess phase is estimated as $\Delta S_I = \overline{S}_2^{ext}(t) - \overline{S}_1(t)$. The corrected L2 excess phase $S_2^{cor}(t)$ below the cut-off point is computed as follows: the finite differences of $S_2^{cor}(t)$ are formed as a linear combination of finite differences of $S_1 + \Delta S_I$ and finite differences of S_2 with weights $W(t)$ and $(1 - W(t))$, respectively [5], where the weighting function $W(t)$ smoothly increases from 0 to 1 in the vicinity of the cut-off point. The L2 amplitude is also multiplied with $(1 - W(t))$ and it is used for the determination of the cut-off point within the CT algorithm.

3.3 Geometric Optical Retrieval of Bending Angles

The geometric optical (GO) retrieval of bending angle uses the standard relations between the Doppler frequency (i.e. the phase derivative), the impact parameter, and bending angle. The computation of the Doppler frequency requires the differentiation of the noisy excess phase, which requires filtering. Because excess phase is a convex function (i.e. has systematically positive 2nd derivative), some filters may result in a systematic error. In particular, UCAR have recently eliminated this effect in their processing (announcements at http://cosmic-

io.cosmic.ucar.edu/cdaac/index.html). To get rid of this effect, we subtract a trend from the excess phase. The trend is computed by means of spline regression with a limited number of nodes. We use 30 nodes, which is significantly smaller than the typical number of samples in one occultation (usually not less than 3000). The resulting spline can be differentiated analytically, and the residual excess phase is differentiated numerically. Our data processing system has two choices of the filter type: the filter described by [8] and the polynomial regression. The latter was used in this study.

3.4 Wave Optical Retrieval of Bending Angles

Our wave optical (WO) retrieval of bending angles has three choices: Back Propagation (BP) [9], Canonical Transform of the 1st type (CT) applied after BP [10], and Canonical Transform of the 2nd type (CT2) applied directly to the measurements of the complex field along the LEO orbit [11]. The latter method combines the numerical efficiency of the Full-Spectrum Inversion (FSI) method [12] and the high accuracy approaching that of the Phase Matching (PM) method [13], which provides the most accurate solution. CT2 is our method of choice and it is applied in this study. WO processing is activated below some height specified by a command-line option. In this study, the height equals 25 km.

The core of the CT2 approach is a transform of the measured complex wave field into the representation of the impact parameter, which is implemented by a Fourier Integral Operator (FIO) of the second kind:

$$\hat{\Phi}_2 u(\tilde{p}) = \sqrt{\frac{-ik}{2\pi}} \int a_2(p,t) \exp\left(ikS_2(p,t)\right) u(t)\, dt, \tag{13}$$

where $u(t)$ is the measured complex wave field, $S_2(p,t)$ is the phase function, $a_2(p,t)$ is the amplitude function, or the symbol of the FIO, and $\hat{\Phi}_2 u(\tilde{p})$ is the wave field in the transformed space.

The exact expressions for the amplitude and phase functions were established in the framework of the PM method [11, 13]. However, the exact operator defies a fast numerical implementation. To reduce the FIO to a composition of a Fourier transform, a non-linear scaling of the coordinate and the superimposing of a phase model, we introduce the representation of the approximate impact parameter. For this purpose, we introduce a smooth model of ray structure without multi-path propagation and linearize the expression for the impact parameter as follows:

$$\begin{aligned} \tilde{p}(t,\sigma) &= p_0(t) + \frac{\partial p_0}{\partial \sigma}\left(\sigma - \sigma_0(t)\right) = f(t) + \frac{\partial p_0}{\partial \sigma}\sigma, \\ f(t) &= p_0(t) - \left.\frac{\partial p_0}{\partial \sigma}\right|_{\sigma=\sigma_0(t)} \sigma_0(t), \end{aligned} \tag{14}$$

where $\tilde{p}(t,\sigma)$ is the approximate impact parameter, $\sigma = d\Psi / dt$ is the momentum corresponding to wave field $u(t) = A(t)\exp\left(ik\Psi(t)\right)$, $\sigma_0(t)$ is a smooth model of the phase, and $p_0(t) = p\left(t, \sigma_0(t)\right)$ is the impact parameter computed for the smooth model of the ray manifold. We introduce a new coordinate Y instead of time and the corresponding momentum η as follows:

$$dY = \left(\frac{\partial p_0}{\partial \sigma}\right)^{-1} dt = \frac{\partial \sigma}{\partial p_0} dt, \qquad \eta = \frac{\partial p_0}{\partial \sigma}\sigma. \tag{15}$$

The canonical transform from (Y,η) to $(\tilde{p},\xi)$, where ξ is the new momentum, can be written in the following form:

$$\tilde{p} = f(Y) + \eta, \qquad \xi = -Y, \tag{16}$$

where $f(Y) \equiv f\left(t(Y)\right)$. The corresponding phase function can the be written as the sum of a bi-linear term and a phase model being a function of Y:

$$S_2(\tilde{p},Y) = -\tilde{p}Y + \int_0^Y f(Y')dY', \tag{17}$$

and $f(t)$ evaluates as follows:

$$f(t) = p_0 - \left(\dot{\theta} - \frac{\dot{r}_G}{r_G}\frac{p_0}{\sqrt{r_G^2 - p_0^2}} - \frac{\dot{r}_L}{r_L}\frac{p_0}{\sqrt{r_L^2 - p_0^2}}\right)^{-1}\sigma_0. \tag{18}$$

The corresponding amplitude function reads [11]:

$$a_2(\tilde{p},Y) = \left(\sqrt{r_L^2 - \tilde{p}^2}\sqrt{r_G^2 - \tilde{p}^2}\left\{\frac{r_L r_G \sin\theta}{\tilde{p}}\right\}_{3D}\right)^{1/2}. \tag{19}$$

Finally, we arrive at the following expression for the FIO projecting the measured wave field into the representation of the approximate impact parameter:

$$\hat{\Phi}_2 u(\tilde{p}) = \sqrt{\frac{-ik}{2\pi}}\, a_2\left(\tilde{p}, Y_s(\tilde{p})\right)\int \exp(-ik\tilde{p}Y)\exp\left(ik\int_0^Y f(Y')dY'\right)u(Y)dY, \tag{20}$$

where $u(Y)$ is understood as $u\left(t(Y)\right)$. We replaced $a_2(\tilde{p},Y)$ by its value $a_2\left(\tilde{p},Y_s(\tilde{p})\right)$ at the stationary point $Y_s(\tilde{p})$ and factored it out from within the integral. Function $Y_s(\tilde{p})$ equals $-\xi(\tilde{p})$, where momentum $\xi(\tilde{p})$ is defined as the derivative of the eikonal of the field $\hat{\Phi}_2 u(\tilde{p})$ in the transformed space. For the computation of the eikonal we first substitute $a_2 \equiv 1$ and evaluate the integral, then evaluate $a_2\left(\tilde{p},Y_s(\tilde{p})\right)$ and multiply the transformed field with it. The bending angle as a function of p is determined from the following relation:

$$\varepsilon(p) = \theta\left(t\left(Y_s(p)\right)\right) - \arccos\frac{p}{r_G\left(t\left(Y_s(p)\right)\right)} - \arccos\frac{p}{r_L\left(t\left(Y_s(p)\right)\right)}. \tag{21}$$

where the satellite radii r_G, r_L (in the system of the Earth's local curvature center) and the satellite-to-satellite angle θ are functions of time t, which can be expressed as a function of Y from (15). Expression (20) allows for a fast numerical implementation based on the FFT.

Our WO processing includes the RH filtering in the impact parameter domain [5]. After the RH filtering the cut-off height is determined from the CT amplitude. For this purpose we determine the maximum of the correlation of the CT amplitude with the step function. RH filtering makes this procedure more stable and improves the quality of the shadow border determination. In the L2 channel, the cut-off height determined from the L2 CT amplitude

corresponds to the L2 cut-off height defined above. Below the L2 cut-off height, the L2 CT bending angle is extrapolated in the same way as in GO processing.

If one of the WO processing options is activated, the bending angles from GO processing and from WO processing steps are merged, producing profiles of L1 and L2 bending angles $\varepsilon_{1,2}(p)$. In the framework of WO processing, we also compute the RH error variances $\left\langle \left(\delta\varepsilon_1^{WO}(p)\right)^2 \right\rangle$ of the bending angles.

3.5 Ionospheric Correction and Noise Reduction

The ionospheric correction and noise reduction follows the Optimal Linear Combination (OLC) technique described by [14]. The computation of the background profile of bending angle has the following options: 1) bending angles computed by Abel integral from the local refractivity profile from MSIS climatology, 2) global search of MSIS bending angle profile [15] (initially suggested by Stig Syndergaard, 1999), and 3) bending angles obtained by Abel integral from the local refractivity profile extracted from global fields of analyses of ECMWF or NCEP in the GRIB format.

When using ECMWF/NCEP global fields the local refractivity profile is computed for the approximate ray perigee locations. For locating the ray perigees we use the local MSIS refractivity and bending angles, due to the following reasons: 1) this provides a sufficient accuracy, 2) MSIS refractivity profile is smooth and free from ducting effects that require special handling.

The upper height of ECMWF/NCEP global fields may reach 70–80 km. Because the background bending angle profile is necessary up to a larger height (150 km in our system), we extrapolate the analysis by adding MSIS profiles multiplied with a fitting coefficient. The coefficient is chosen such that the integration of the hydrostatic equation should result in correct MSIS/NCEP temperatures.

When using the MSIS climatology, locally or from the global search, the profile of bending angle is subject to 1-parameter [14] or 2-parameter [16] fitting. Given the model profile $\varepsilon_M(p)$, it is replaced by $\alpha\varepsilon_M(p)$ or $\alpha\left[\varepsilon_M(p)\right]^\beta$, the coefficients α and β being determined from regression of $\varepsilon_M(p)$ with respect to the linear combination $\varepsilon_{LC}(p)$ of L1 and L2 bending angle profiles. Linear combination $\varepsilon_{LC}(p)$ contains the ionospheric noise and it is referred to as the raw bending angle profile. In this study we used 2-parameter fitting in the 20–70 km height interval.

OLC procedure produces the neutral bending angle $\varepsilon(p)$ and its error variances $\left\langle \left(\delta\varepsilon^{OLC}(p)\right)^2 \right\rangle$. Finally, we create a merged profile of bending angle consisting of $\varepsilon(p)$ in the height range where RO data are present and extended up to 150 km by the background profile $\alpha\left[\varepsilon_M(p)\right]^\beta$. We also obtain the profile of the error variances $\left\langle \left(\delta\varepsilon^{OLC}(p)\right)^2 \right\rangle + \left\langle \left(\delta\varepsilon_1^{WO}(p)\right)^2 \right\rangle$.

3.6 Inversion of Bending Angles

The retrieval of refractivity and dry temperatures follows the standard procedure based on the Abel inversion. Using the error variance of the bending angle, we also retrieve the error variances of refractivity and dry temperature [17].

4. Examples of Processing

In the processing of GRAS data we observe all the typical features that we can also see in COSMIC data: multipath structures and reflected rays.

Below we present diagnostic plots for selected cases. The plots have 9 panels organized as table with 3 rows and 3 columns.

The left panel in the upper row shows amplitudes (red line) and receiver mode (blue line, 0 for CL, 750 for RS). The middle panel in the upper raw shows bending angles: L1 from GO processing (black line, GO L1), L2 from GO processing (red line, GO L2), and ionospherically-corrected neutral atmospheric bending angle from CT (green line, CT N). The right panel in the upper raw shows bending angles for large heights: ionospheric (blue line, IONO), linear combination of L1 and L2 (red line, LC), neutral bending angle from CT (green line, CT N).

The left panel in the middle raw shows tropospheric bending angles and receiver mode: GO L1 (black line), GO L2 (red line), CT L1 (green line), CT L2 (blue line), and the border between the CL and RS receiver modes in the bending angle – impact parameter space (violet line, CL/RS). The middle panel in the middle raw shows the CT amplitude. The right panel in the middle raw shows the L1 radio-holographic spectra in the troposphere and CT L1 bending angles (red line).

The left panel in the lower raw indicates the L1 radio-holographic spectra up to a height of 30 km. The middle panel in the lower raw indicates the L2 radio-holographic spectra up to a height of 30 km. The right panel in the lower raw indicates the retrieved dry temperature profile.

4.1 Processing of CL+RS Data

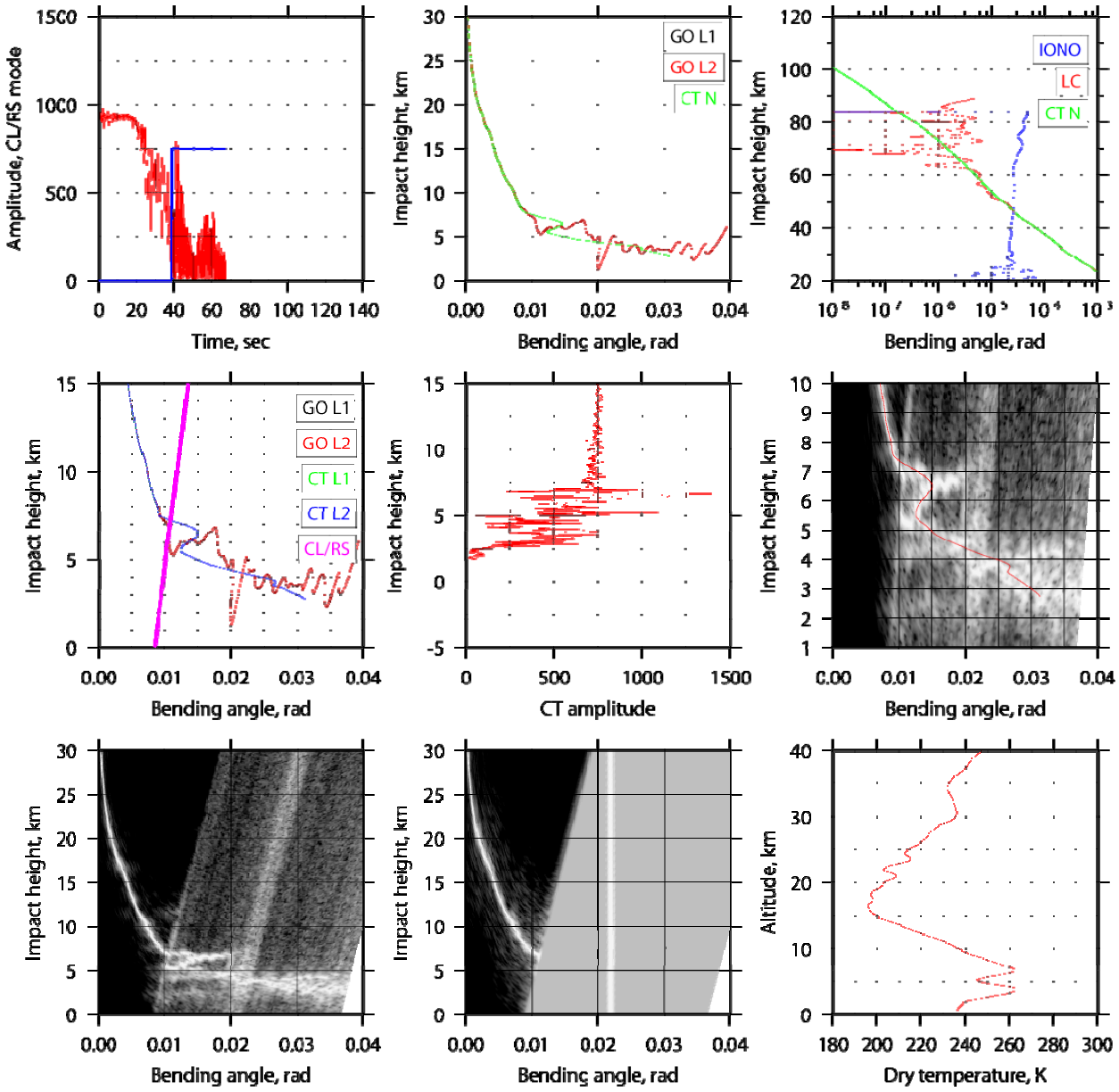

Figure 3. Occultation event observed on 2007/09/30 at UTC 00:12, 4.7°S 25.3°W, badness score 28.102. This is an example of a tropical event with a pronounced multipath structure.

Figure 3 shows an example of a tropical occultation with a pronounced multipath structure. The interfering rays are observed in the impact parameter range of 5–7 km. The CT amplitude indicates strong scintillations which are typical for a turbulent atmosphere. The multipath structure must originate from a strong humidity layer located at a height of 5 km. This is a setting event. The receiver switched to the RS mode at a height of 7 km.

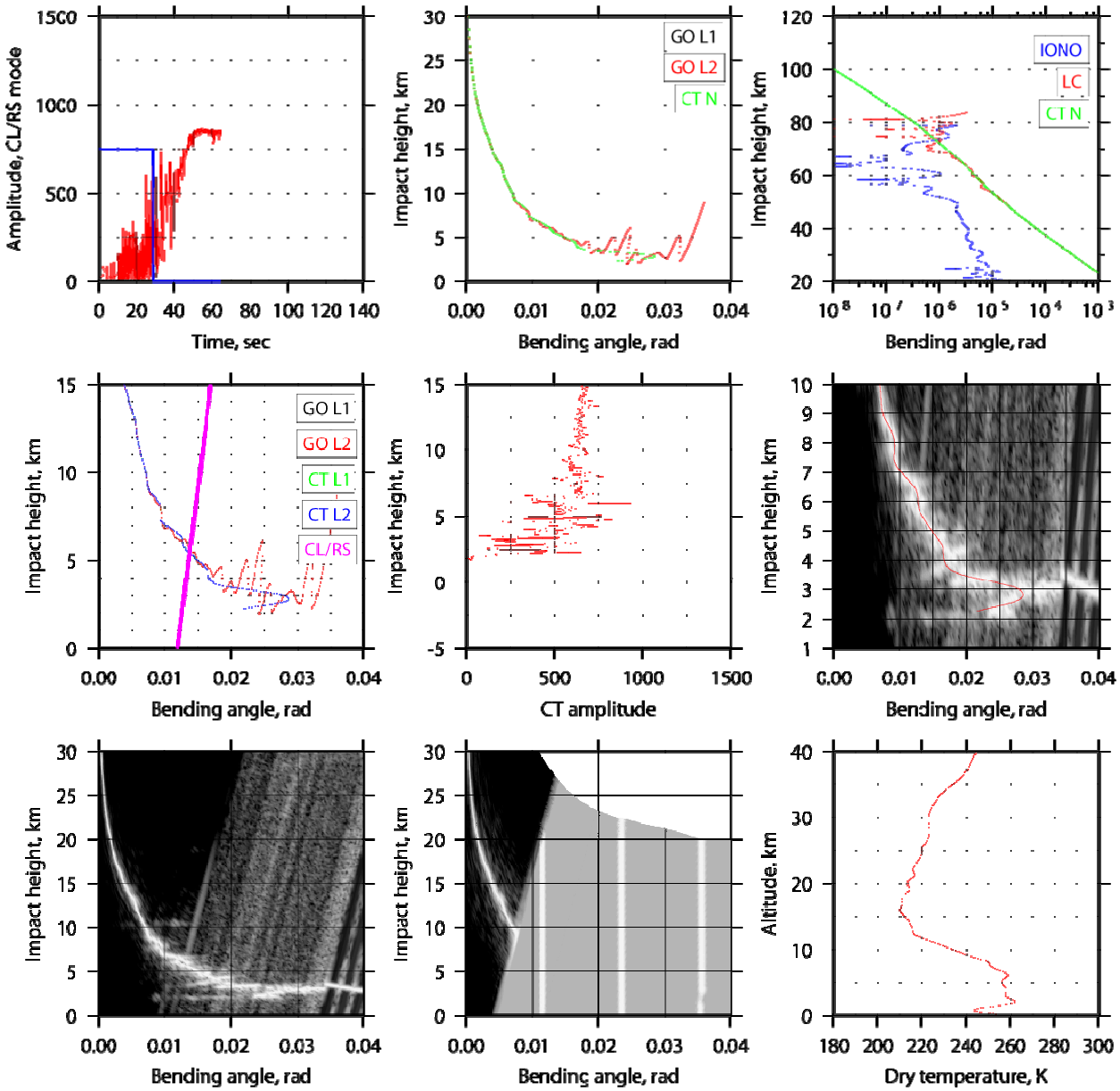

Figure 4. Occultation event observed on 2007/09/30 at UTC 00:13, 46.1°N 57.7°W, badness score 26.499. This is an example of a middle-latitude event with medium-strength multipath effects.

Figure 4 shows an example of a middle-latitude occultation. Here we observe multipath effects of medium strength. The CT amplitude also indicates scintillations, but they have lower spatial frequencies signifying a different type of structures as compared to the above tropical example. This is a rising event. In the deep shadow the RS record indicates multiple long gaps separated by short pieces of data. This is explained by the fact that receiver repeatedly attempted to lock the signal. The spectra also show the rough phase model, which was used to fill-in the gaps. This part of the record was cut-off in the inversion. The receiver left the RS mode and switched to CL at a height of 6 km.

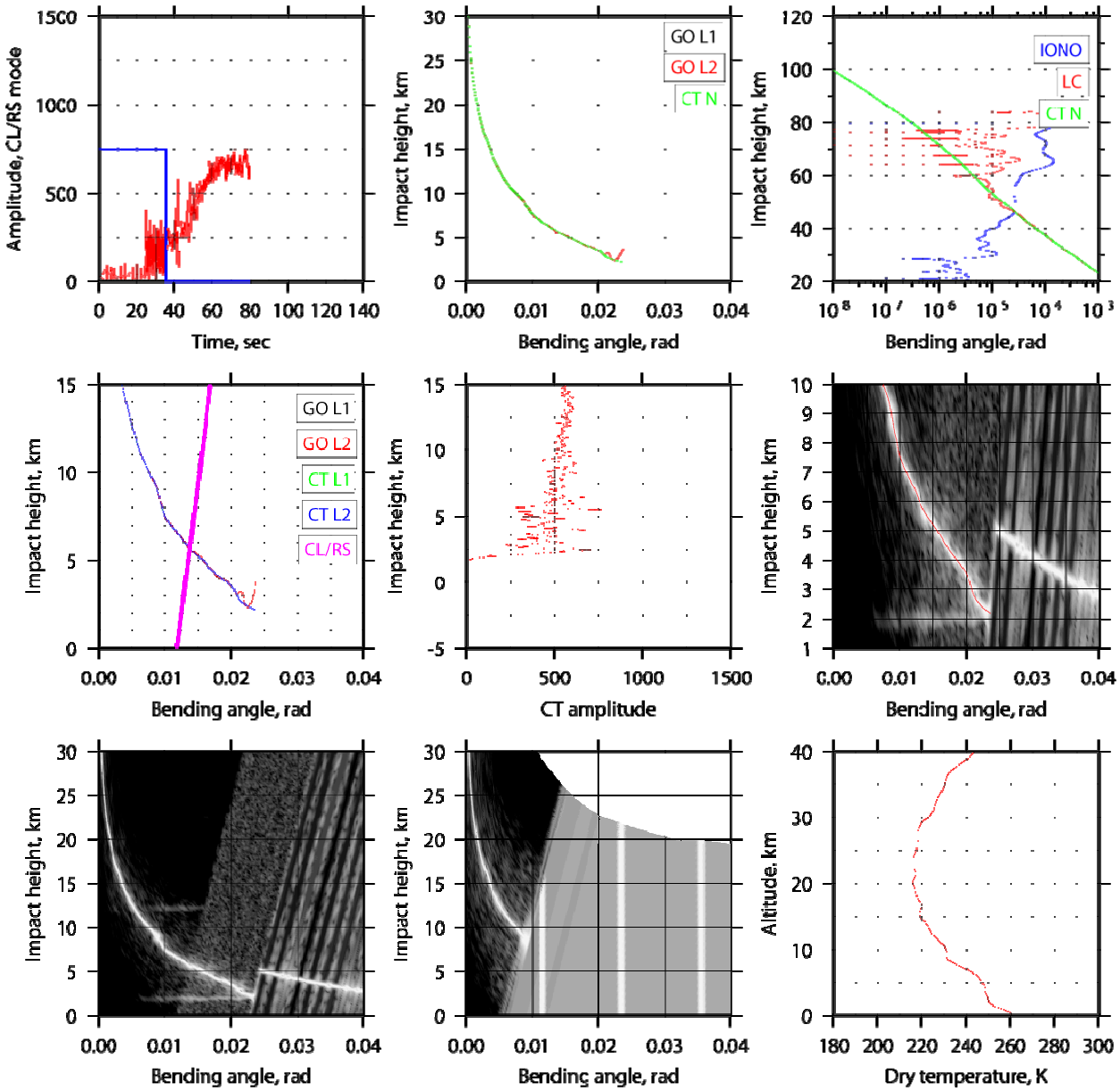

Figure 5. Occultation event observed on 2007/09/30 at UTC 00:17, 60.2°N 47.2°W, badness score 18.904. This is an example of polar occultation with a pronounced reflected ray.

Figure 5 show an example of a polar occultation event observed in the Arctic. This example indicates multipath effects due to the reflected ray. This is a rising event. We see the gaps similar to those in the previous example. The receiver left the RS mode and switched to CL at a height of 5.5 km.

4.2 Processing of CL Data

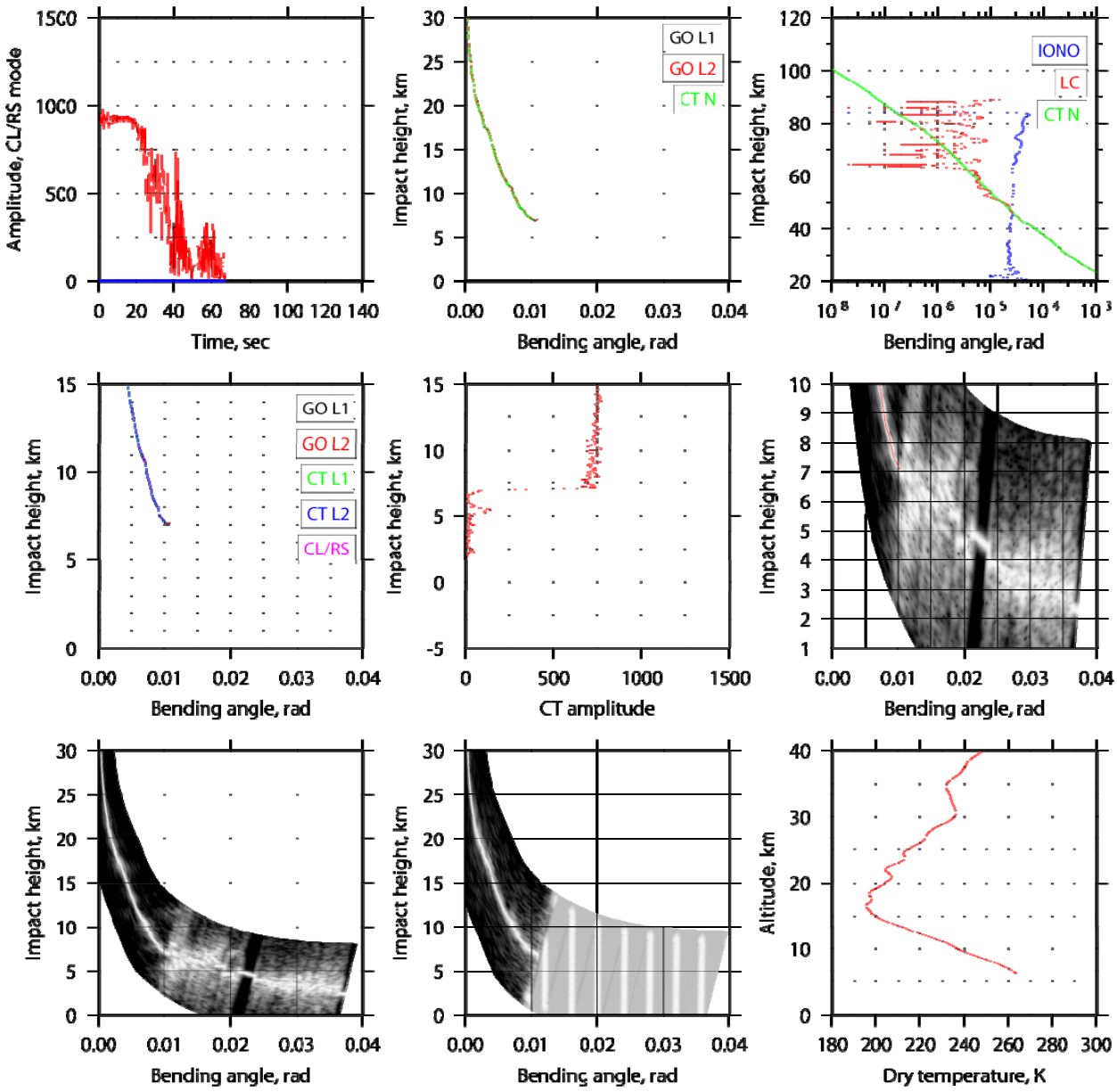

Figure 6. Occultation event observed on 2007/09/30 at UTC 00:12, 4.7°S 25.3°W, badness score 22.859. This is an example of a tropical event with a pronounced multipath structure.

Figure 6 shows the same occultation event as in Figure 3, but processed using CL data only. The multipath structure in the spectra is not well-reproduced. The data indicate multiple gaps, one of which is located just before the beginning of the multipath structure. Due to that, the retrieval does not penetrate below 7 km.

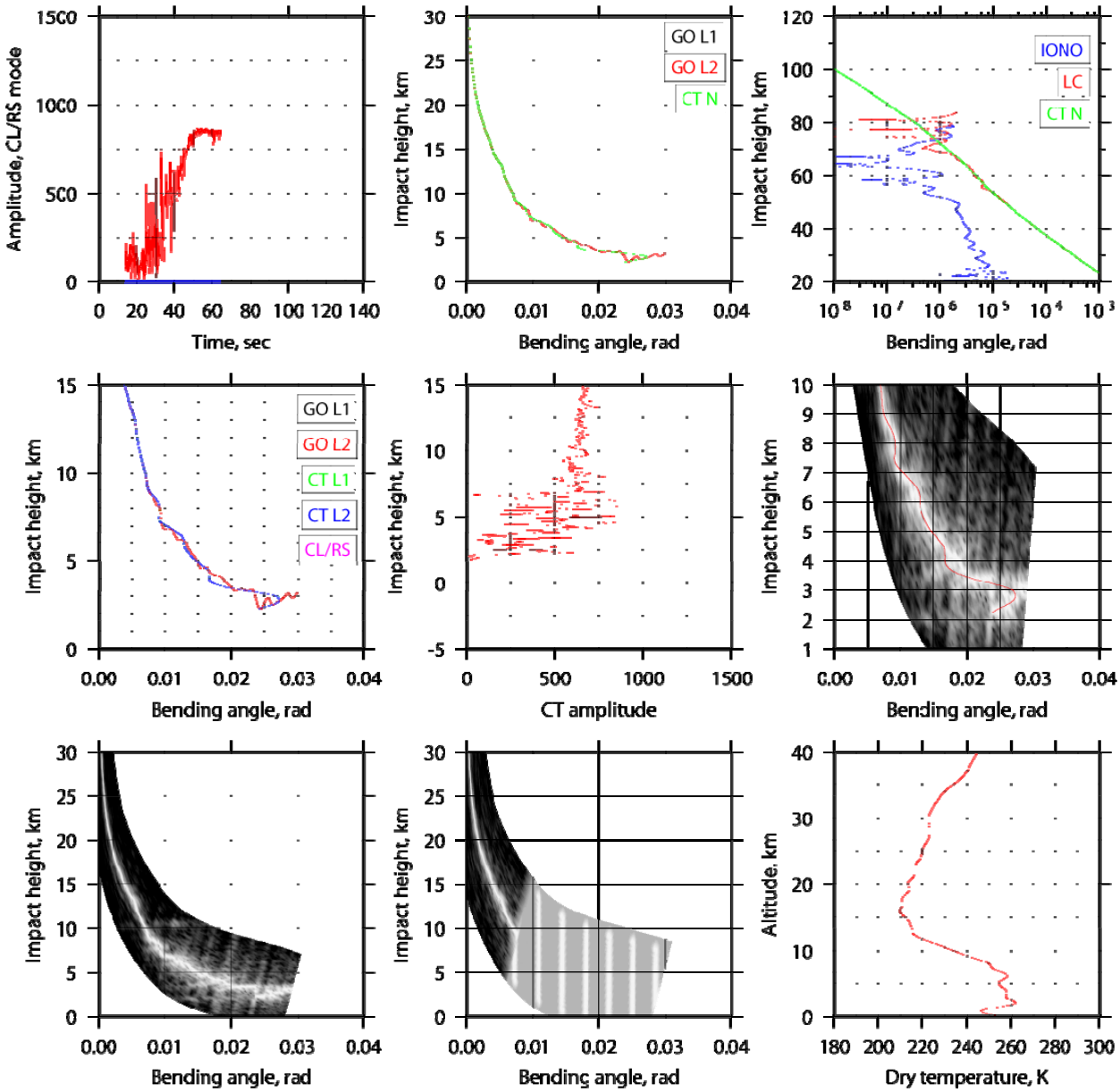

Figure 7. Occultation event observed on 2007/09/30 at UTC 00:13 46.1°N 57.7°W, badness score 26.499. This is an example of a middle-latitude event with medium-strength multipath effects.

Figure 7 shows the same occultation event as in Figure 4, but processed using CL data only. Here the multipath structure is reproduced correctly, but the spectra indicate a higher level of noise.

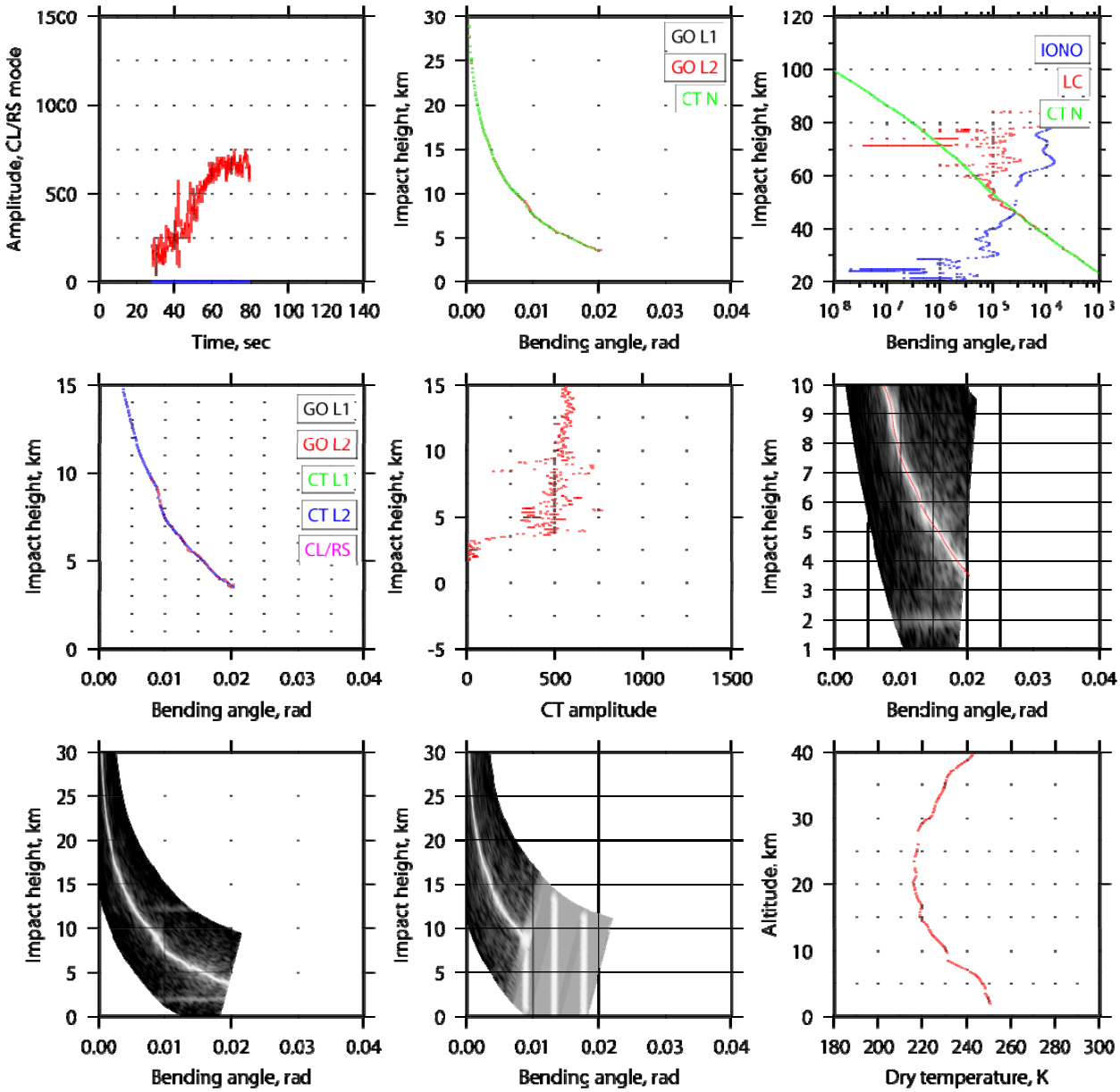

Figure 8. Occultation event observed on 2007/09/30 at UTC 00:17, 60.2°N 47.2°W, badness score 18.904. This is an example of polar occultation with a pronounced reflected ray.

Figure 8 shows the same occultation event as in Figure 5, but processed using CL data only. CL data reproduce the reflected ray, but have a poorer penetration. The retrieval begins at a height of 3.5 km, unlike the RS data, where it starts at the surface.

5. References

1. Sokolovskiy, S., Y.-H. Kuo, C. Rocken, W. S. Schreiner, D. Hunt, and R. A. Anthes, Monitoring the atmospheric boundary layer by GPS radio occultation signals recorded in the open-loop mode, Geophys. Res. Lett., 33, L12,813, doi:10.1029/2006GL025,955, 2006.
2. Sokolovskiy, S., C. Rocken, W. Schreiner, D. Hunt, and J. Johnson, Postprocessing of L1 GPS radio occultation signals recorded in open-loop mode, Radio Science, 44, RS2002, doi:10.1029/2008RS003,907, 2009.
3. Beyerle, G., M. E. Gorbunov, and C. O. Ao, Simulation studies of GPS radio occultation measurements, Radio Sci., 38, 1084, doi: 10.1029/2002RS002,800, 2003.
4. Ziedan, N. I., GNSS Receivers for Weak Signals, Artech House, Norwood, Mass., 2006.
5. Gorbunov, M. E., K. B. Lauritsen, A. Rhodin, M. Tomassini, and L. Kornblueh, Radio holographic Filtering, error estimation, and quality control of radio occultation data, Journal of Geophysical Research, 111, D10,105, doi: 10.1029/2005JD006,427, 2006.
6. Kuo, Y., T. Wee, S. Sokolovskiy, C. Rocken, W. Schreiner, D. Hunt, and R. Anthes, Inversion and error estimation of GPS radio occultation data, J. Meteor. Soc. Japan, 82, 507–531, 2004a.
7. Beyerle, G. S., J. Wickert, T. Schmidt, and C. Reigber, Atmospheric sounding by global navigation satellite system radio occultation: An analysis of the negative refractivity bias using CHAMP observations, J. Geophys. Res., 109, doi:10.1029/2003JD003,922, 2004.
8. Ustinvov, E. A., To the solution of the problem of the numerical differentiation by the statistical optimization method, Cosmic Research (Kosmicheskie issledovaniya), 28, 545–554, 1990, in Russian.
9. Gorbunov, M. E., and A. S. Gurvich, Microlab-1 experiment: Multipath effects in the lower troposphere, Journal of Geophysical Research, 103, 13,819–13,826, 1998.
10. Gorbunov, M. E., Canonical transform method for processing GPS radio occultation data in lower troposphere, Radio Sci., 37, 9-1–9-10, doi:10.1029/2000RS002,592, 2002a.
11. Gorbunov, M. E., and K. B. Lauritsen, Analysis of wave fields by Fourier Integral Operators and its application for radio occultations, Radio Sci., 39, RS4010, doi:10.1029/2003RS002,971, 2004.
12. Jensen, A. S., M. S. Lohmann, H.-H. Benzon, and A. S. Nielsen, Full spectrum inversion of radio occultation signals, Radio Sci., 38, 6-1–6-15, doi: 10.1029/2002RS002,763, 2003.
13. Jensen, A. S., M. S. Lohmann, A. S. Nielsen, and H.-H. Benzon, Geometrical optics phase matching of radio occultation signals, Radio Sci., 39, RS3009, doi: 10.1029/2003RS002,899, 2004.
14. Gorbunov, M. E., Ionospheric correction and statistical optimization of radio occultation data, Radio Sci., 37, 17-1–17-9, doi: 10.1029/2000RS002,370, 2002b.
15. Gobiet, A., and G. Kirchengast, Advancements of Global Navigation Satellite System radio occultation retrieval in the upper stratosphere for optimal climate monitoring utility, Journal of Geophysical Research, 109, D24,110, doi:10.1029/2004JD005,117, 2004.
16. Lohmann, M. S., Analysis of global positioning system (GPS) radio occultation measurement errors based on Satellite de Aplicaciones Cientificas-C (SAC-C) GPS radio occultation data recorded in open-loop and phase-locked-loop mode, J. of Geophys. Res., 112, D09,115, doi:10.1029/2006JD007,764, 2007.

17. Gorbunov, M. E., K. B. Lauritsen, A. Rodin, M. Tomassini, and L. Kornblueh, Analysis of the CHAMP experimental data on radio-occultation sounding of the Earth's atmosphere, Izvestiya, Atmospheric and Oceanic Physics, 41,726–740,2005.
18. Lohmann, M. S., Dynamic Error Estimation for Radio Occultation Bending Angles Retrieved by the Full Spectrum Inversion Technique, Radio Science, 2006, 41, RS5005, doi:10.1029/2005RS003396.
19. M. S. Lohmann, Application of Dynamical Error Estimation for Statistical Optimization of Radio Occultation Bending Angles, Radio Science, 2005, 40, RS3011, doi:10.1029/2004RS003117.
20. Kursinski, E. R., S. B. Healy, and L. J. Romans, Initial Results of Combining GPS Occultations with ECMWF Global Analyses Within a 1DVar Framework, Earth Planets Space 52 (11) pp. 885-892 (2001).
21. Sokolovskiy, S., W. Schreiner, C. Rocken, and D. Hunt, Optimal Noise Filtering for the Ionospheric Correction of GPS Radio Occultation Signals, Journal of Atmospheric and Oceanic Technology, 2009, 26, July, 1398–1403.

6. Appendix. Definitions of GRAS NetCDF Variables

6.1 Dimensions

Name	Explanation	Example value
dim_unlim	Unlimited dimension (currently not used)	UNLIMITED // (0 currently)
dim_xyz	Spatial dimension	3
dim_CCCC	Closed loop (CL) data (name includes CCCC – amount of CL data)	3065
dim_RRRRR	Raw sampling (RS) data (name includes RRRRR – amount of RS data)	24460

6.2 Variables

Type	Name	Dimensions	Explanation	Units
int	Prn		PRN number of the occulting GNSS satellite	
int	channel		GRAS channel on which the occultation was measured	
int	start_time_absdate		Start (reference) time for all observation epochs / date	days since 0001-01-01 00:00:00.00
double	start_time_abstime		Start (reference) time for all observation epochs / time	seconds since 00:00:00.00
double	longitude		Longitude (for SLTA = 0)	degrees_east
double	latitude		Latitude (for SLTA = 0)	degrees_north
double	azimuth		Azimuth angle (for SLTA = 0)	degrees
byte	have_cl_data		True if closed loop data is available	
byte	have_rs_data		True if raw sampling data is available	
byte	have_continuous_cl_rs		True if closed loop and raw sampling data form continuous time series	
double	cl_dtime	(dim_CCCC)	Measurement epoch	seconds since start of event

Type	Name	Dimensions	Explanation	Units
double	cl_slta	(dim_CCCC)	Straight line tangent altitude	meters
double	cl_r_gns	(dim_CCCC, dim_xyz)	J2000 position of occulting GNSS satellite (centre of mass)	meters
double	cl_v_gns	(dim_CCCC, dim_xyz)	J2000 velocity of occulting GNSS satellite (centre of mass)	meters/second
double	cl_r_rec	(dim_CCCC, dim_xyz)	J2000 position of receiving GRAS antenna (phase centre)	meters
double	cl_v_rec	(dim_CCCC, dim_xyz)	J2000 velocity of receiving GRAS antenna (phase centre)	meters/second
double	cl_phase_l1_nco	(dim_CCCC)	L1 carrier NCO phase	meters
double	cl_phase_l2_nco	(dim_CCCC)	L2 carrier NCO phase	meters
double	cl_phase_ca	(dim_CCCC)	C/A carrier phase including I/Q contributions	meters
double	cl_phase_p1	(dim_CCCC)	P1 carrier phase including I/Q contributions	meters
double	cl_phase_p2	(dim_CCCC)	P2 carrier phase including I/Q contributions	meters
double	cl_exphase_l1_nco	(dim_CCCC)	L1 carrier NCO excess phase	meters
double	cl_exphase_l2_nco	(dim_CCCC)	L2 carrier NCO excess phase	meters
double	cl_exphase_ca	(dim_CCCC)	C/A carrier excess phase including I/Q contributions	meters
double	cl_exphase_p1	(dim_CCCC)	P1 carrier excess phase including I/Q contributions	meters
double	cl_exphase_p2	(dim_CCCC)	P2 carrier excess phase including I/Q contributions	meters
double	cl_i_ca_cnts_raw	(dim_CCCC)	In-phase component I of C/A carrier phase measurements	counts

Type	Name	Dimensions	Explanation	Units
double	cl_i_ca_cnts	(dim_CCCC)	In-phase component I of C/A carrier phase measurements, navigation bits demodulated	counts
double	cl_i_p1_cnts	(dim_CCCC)	In-phase component I of P1 carrier phase measurements	counts
double	cl_i_p2_cnts	(dim_CCCC)	In-phase component I of P2 carrier phase measurements	counts
double	cl_q_ca_cnts_raw	(dim_CCCC)	Quadrature component Q of C/A carrier phase measurements	counts
double	cl_q_ca_cnts	(dim_CCCC)	Quadrature component Q of C/A carrier phase measurements, navigation bits demodulated	counts
double	cl_q_p1_cnts	(dim_CCCC)	Quadrature component Q of P1 carrier phase measurements	counts
double	cl_q_p2_cnts	(dim_CCCC)	Quadrature component Q of P2 carrier phase measurements	counts
double	cl_i_ca_uncorr	(dim_CCCC)	In-phase component I of C/A carrier phase measurements, normalized to antenna port	V
double	cl_i_ca	(dim_CCCC)	In-phase component I of C/A carrier phase measurements, navigation bits demodulated, normalized to antenna port	V

Type	Name	Dimensions	Explanation	Units
double	cl_i_p1	(dim_CCCC)	In-phase component I of P1 carrier phase measurements, normalized to antenna port	V
double	cl_i_p2	(dim_CCCC)	In-phase component I of P2 carrier phase measurements, normalized to antenna port	V
double	cl_q_ca_uncorr	(dim_CCCC)	Quadrature component Q of C/A carrier phase measurements, normalized to antenna port	V
double	cl_q_ca	(dim_CCCC)	Quadrature component Q of C/A carrier phase measurements, navigation bits demodulated, normalized to antenna port	V
double	cl_q_p1	(dim_CCCC)	Quadrature component Q of P1 carrier phase measurements, normalized to antenna port	V
double	cl_q_p2	(dim_CCCC)	Quadrature component Q of P2 carrier phase measurements, normalized to antenna port	V
double	cl_amplitude_ca	(dim_CCCC)	Amplitude of C/A carrier phase measurements, normalized to antenna port	V
double	cl_amplitude_p1	(dim_CCCC)	Amplitude of P1 carrier phase measurements, normalized to antenna port	V

Type	Name	Dimensions	Explanation	Units
double	cl_amplitude_p2	(dim_CCCC)	Amplitude of P2 carrier phase measurements, normalized to antenna port	V
double	cl_snr_ca	(dim_CCCC)	Signal-to-Noise-Ratio of C/A carrier phase measurements	V/V
double	cl_snr_p1	(dim_CCCC)	Signal-to-Noise-Ratio of P1 carrier phase measurements	V/V
double	cl_snr_p2	(dim_CCCC)	Signal-to-Noise-Ratio of P2 carrier phase measurements	V/V
double	cl_snr_ca_mean		Mean Signal-to-Noise-Ratio of C/A carrier phase measurements (SLTA > 60 km)	V/V
double	cl_snr_p1_mean		Mean Signal-to-Noise-Ratio of P2 carrier phase measurements (SLTA > 60 km)	V/V
double	cl_snr_p2_mean		Mean Signal-to-Noise-Ratio of P2 carrier phase measurements (SLTA > 60 km)	V/V
double	cl_noise_power_l1_mean		Mean noise power spectral density for L1 phase measurements	db/Hz
double	cl_noise_power_l2_mean		Mean noise power spectral density for L2 phase measurements	db/Hz
double	cl_exphase_ca_noise		Mean phase noise of C/A carrier excess phase measurements (SLTA > 60 km)	meters
double	cl_exphase_p1_noise		Mean phase noise of P1 carrier excess phase measurements (SLTA > 60 km)	meters

Type	Name	Dimensions	Explanation	Units
double	cl_exphase_p2_noise		Mean phase noise of P2 carrier excess phase measurements (SLTA > 60 km)	meters
double	cl_slta_main_ca_min		Minimum SLTA of main C/A carrier phase data segment	meters
double	cl_slta_main_ca_max		Maximum SLTA of main C/A carrier phase data segment	meters
double	cl_slta_main_p1_min		Minimum SLTA of main P1 carrier phase data segment	meters
double	cl_slta_main_p1_max		Maximum SLTA of main P1 carrier phase data segment	meters
double	cl_slta_main_p2_min		Minimum SLTA of main P2 carrier phase data segment	meters
double	cl_slta_main_p2_max		Maximum SLTA of main P2 carrier phase data segment	meters
double	cl_navbits_external	(dim_CCCC)	External navigation data bits (if available)	
double	cl_navbits_internal	(dim_CCCC)	Internal navigation data bits	
int	cl_tracking_state	(dim_CCCC)	Tracking states	
byte	cl_have_navbits_external		True if external navigation bit data available and used during processing	
byte	cl_snr_ca_ok		True if mean C/A carrier phase SNR > 200 V/V (SLTA > 60 km)	
byte	cl_snr_p1_ok		True if mean P1 carrier phase SNR > 200 V/V (SLTA > 60 km)	
byte	cl_snr_p2_ok		True if mean P2 carrier phase SNR > 200 V/V (SLTA > 60 km)	

Type	Name	Dimensions	Explanation	Units
double	cl_clk_gns	(dim_CCCC)	Clock bias of the occulting GNSS satellite	seconds
double	cl_clk_rec	(dim_CCCC)	Clock bias of the GRAS receiver	seconds
double	cl_phase_l1_nco_undiff	(dim_CCCC)	L1 carrier NCO phase (undifferenced)	meters
double	cl_phase_l2_nco_undiff	(dim_CCCC)	L2 carrier NCO phase (undifferenced)	meters
double	rs_dtime	(dim_RRRRR)	Measurement epoch	seconds since start of event
double	rs_slta	(dim_RRRRR)	Straight line tangent altitude	meters
double	rs_r_gns	(dim_RRRRR, dim_xyz)	J2000 position of occulting GNSS satellite (centre of mass)	meters
double	rs_v_gns	(dim_RRRRR, dim_xyz)	J2000 velocity of occulting GNSS satellite (centre of mass)	meters/second
double	rs_r_rec	(dim_RRRRR, dim_xyz)	J2000 position of receiving GRAS antenna (phase centre)	meters
double	rs_v_rec	(dim_RRRRR, dim_xyz)	J2000 velocity of receiving GRAS antenna (phase centre)	meters/second
double	rs_phase_l1_nco	(dim_RRRRR)	L1 carrier NCO phase	meters
double	rs_phase_ca	(dim_RRRRR)	C/A carrier phase including I/Q contributions	meters
double	rs_exphase_l1_nco	(dim_RRRRR)	L1 carrier NCO excess phase	meters
double	rs_exphase_ca	(dim_RRRRR)	C/A carrier excess phase including I/Q contributions	meters
double	rs_i_ca_cnts_raw	(dim_RRRRR)	In-phase component I of C/A carrier phase measurements	counts

Type	Name	Dimensions	Explanation	Units
double	rs_i_ca_cnts	(dim_RRRRR)	In-phase component I of C/A carrier phase measurements, navigation bits demodulated	counts
double	rs_q_ca_cnts_raw	(dim_RRRRR)	Quadrature component Q of C/A carrier phase measurements	counts
double	rs_q_ca_cnts	(dim_RRRRR)	Quadrature component Q of C/A carrier phase measurements, navigation bits demodulated	counts
double	rs_i_ca_uncorr	(dim_RRRRR)	In-phase component I of C/A carrier phase measurements, normalized to antenna port	V
double	rs_i_ca	(dim_RRRRR)	In-phase component I of C/A carrier phase measurements, navigation bits demodulated, normalized to antenna port	V
double	rs_q_ca_uncorr	(dim_RRRRR)	Quadrature component Q of C/A carrier phase measurements, normalized to antenna port	V
double	rs_q_ca	(dim_RRRRR)	Quadrature component Q of C/A carrier phase measurements, navigation bits demodulated, normalized to antenna port	V
double	rs_amplitude_ca	(dim_RRRRR)	Amplitude of C/A carrier phase measurements, normalized to antenna port	V

Type	Name	Dimensions	Explanation	Units
double	rs_snr_ca	(dim_RRRRR)	Signal-to-Noise-Ratio of C/A carrier phase measurements	V/V
double	rs_snr_ca_mean		Mean Signal-to-Noise-Ratio of C/A carrier phase measurements (SLTA > 60 km)	V/V
double	rs_noise_power_l1_mean		Mean noise power spectral density for L1 phase measurements	db/Hz
double	rs_slta_main_ca_min		Minimum SLTA of main C/A carrier phase data segment	meters
double	rs_slta_main_ca_max		Maximum SLTA of main C/A carrier phase data segment	meters
double	rs_navbits_external	(dim_RRRRR)	External navigation data bits (if available)	
double	rs_navbits_internal	(dim_RRRRR)	Internal navigation data bits	
int	rs_tracking_state	(dim_RRRRR)	Tracking states	
byte	rs_have_navbits_external		True if external navigation bit data available and used during processing	
byte	rs_snr_ca_ok		True if max C/A carrier phase SNR > 200 V/V	
double	rs_clk_gns	(dim_RRRRR)	Clock bias of the occulting GNSS satellite	seconds
double	rs_clk_rec	(dim_RRRRR)	Clock bias of the GRAS receiver	seconds
double	rs_phase_l1_nco_undiff	(dim_RRRRR)	L1 carrier NCO phase (undifferenced)	meters

6.3 Global attributes:

Name	Example value
title	"MetOp-A / GRAS radio occultation data"
institution	"EUMETSAT"
processing_centre	"EUMETSAT"
processing_time	"2009-02-27 141925.00"
software_version	"0.2.0.dev-r40"
format_version	"0.2.0.dev-r40"
OCC_type	"setting"
pod_method	"BHN"
phase_method	"zero differencing"